

Rail surface crack initiation analysis using multi-scale coupling approach

Y. Ma, V.L. Markine, A.A. Mashal

Section of Railway Engineering, Faculty of Civil Engineering and Geosciences, Delft University of Technology, Delft, The Netherlands

ABSTRACT: A concurrent multi-scale computational strategy for rail surface crack initiation analysis is introduced in current paper. It attempts to take advantage of the efficiency of macroscopic models and the accuracy of the mesoscopic models. The solving procedure is , through the coupling of individual approaches, beginning from the largest scale to the smaller scale, making use of multi-body dynamic(MBS) simulation, explicit finite element(FEM) analysis, sub-modelling technique as well as crack initiation analysis. The main idea of the seamless handshaking algorithms at the interface of the respective approaches is presented. A unified description of crack initiation analysis is built up by linking the models at different scales. Moreover, the surface and sub-surface stress/strain distributions under the wheel-rail rolling contact loads are obtained from coupled simulations. Based on the stress/strain response, the critical plane orientation of surface crack initiation is predicted. It can be concluded that the proposed numerical procedure can provide much accurate and realistic outcomes for rail surface crack initiation analysis in comparison with performing an simulation only on one scale level.

1 INTRODUCTION

Crack-like defects such as “Head-check(HC)” and “squat”, are frequently observed in rails under repeated rolling/sliding contact loads(Dubourg and Lamacq, 2002). The cracks may continue to propagate branching downwards in rails until rupture occurs, or upwards to give rise to a flake, which is detrimental for the railway structural health and safety. For this reason, it is important to investigate the crack growth mechanisms in order to prevent serious consequences of cracks. In this paper, a numerical strategy is developed to investigate cracks with the aim of identifying the initial crack orientation.

The idea of performing crack prediction analysis has obvious appeal as a tool for understanding the damage mechanism and thus making better maintenance schedule. In the past decades, although there has been done extensive research on crack analysis, classical approach on this problem had to deal with major limitations. For example, in predicting fatigue life of rails and wheels (Desimone et al., 2006, Ekberg et al., 2002), simple engineering formulas are commonly utilized together with Multibody system(MBS) analysis. However, due to the assumption of rigid components and elastic material behaviour in MBS simulation, a continuum approach, Finite element method(FEM) cooperating with advanced fatigue life models(Liu et al., 2006, Ringsberg et al., 2000, Sraml et al., 2003) is often employed to do crack initiation/propagation analysis because of its striking versatility. In FEM analysis, material behaviour can be described by sophisticated elasto-plastic models. Besides, dynamic responses and realistic contact geometries can be taken into account as well. Nevertheless, the mesh size

of such FE models is not allowed to be refined to a desired level for crack initiation analysis resulting from the fact that the dimensions of wheels and rails are considerably bigger than the ones of the crack. A study in(Liu et al., 2006) introduced a sub-modelling technique into fatigue life prediction on wheels to overcome this problem. While the feasibility of sub-modelling technique on W/R rolling contact analysis has not yet been verified. Moreover, quasi static loads instead of dynamic loads are applied on the sub-model, which is questionable for the accuracy and effectiveness of sub-modelling approach.

In order to overcome the above mentioned restrictions, a multi-scale coupling approach for rail surface crack initiation analysis is proposed in current study. This paper is organized as follows: the main procedure of computational multi-scale coupling strategy is presented in section 2, which is followed by wheel-rail interaction analysis in macro scale and mesoscale. Moreover, crack initiation analysis will be demonstrated in section 4. Finally, concluding remarks will be presented.

2 COMPUTATIONAL MULTI-SCALE COUPLING STRATEGY

In many problems related to material science, the interactions among ultimate microscopic constituents of materials determine the behavior of the material at macroscopic scale(Lu and Kaxiras, 2004). In order to capture the multi-scale behavior present at a material, numerous multi-scale modelling approaches has been proposed to fulfill different purpose of engineering applications(Li et al., 2010, Yang et al., 2014, Bertolino et al., 2007). However, in the research field of railway engineering, few investigations on wheel-rail interaction using multi-scale approach have been reported so far.

2.1 *Multi-scale definition*

In the context of simulations on wheel-rail interaction, different idealizations and numerical approaches are used to model its response behaviour under variable length scale, wherein one can distinguish four characteristic length levels:

1) Complete macro-scale – vehicle-track interaction, built with MBS model, where a complete vehicle-track system as shown in figure 1(a) is considered and the length of the track normally can be ranged from one to a couple of kilometres.

2) Component macro-scale – wheel/rail components interaction denoted as figure 1 (b), where the dimensions of the wheel and rail model is limited to the order of meter. In this scale, explicit FEM method is routinely utilized to examine the dynamic response between two contact bodies. Sophisticated constitutive laws instead of rigid or elastic assumptions made in MBS simulation, are always employed to describe the material behaviour of the physical system.

3) Mesoscopic scale – rail FEM sub-model as shown in figure 1(c), in which the study on surface initiated crack can be implemented at a desired mesh refining level in the order of 0.1mm. The crack initiation mechanism resulting from dislocations, grain boundaries, and other microstructural defects are able to be unveiled by running the sub-model simulations.

4) Microscopic scale (in the order of a few micro-meters as shown in figure 1(d)) goes one step further, where atoms are the major players and their interactions can be highlighted by classical interatomic potentials(Lu and Kaxiras, 2004). Herein, our study is only limited from macroscopic to mesoscopic scales, the micro-scale analysis is beyond the scope of this research.

Since none of the methods alone would suffice to describe the entire wheel-rail contact system, the goal becomes to develop a coupled macroscopic-to-mesoscopic computational approach which means coupling different methods specialized at different length scales, effectively distributing the computational power where it is needed the most, as well as taking advantage of the efficiency of macroscopic models and the accuracy of the mesoscopic models.

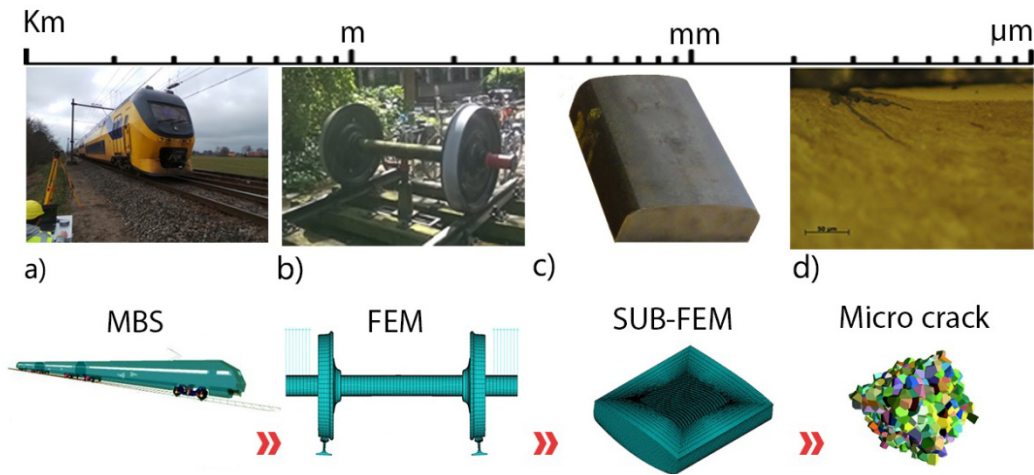


Figure 1. Schematic graph of multi-scale coupling strategy for crack initiation analysis. a) Complete macro scale –vehicle/track interaction; b) Component macro scale – wheel/rail interaction; c) Mesoscale – Rail sub-model crack initiation analysis; d) Micro scale – Rail micro-crack analysis(Franklin et al., 2011, Steenbergen and Dollevoet, 2013).

2.2 Interface handshaking algorithm

Conceptually, two categories of multi-scale simulations can be envisioned, sequential and concurrent. The differences between the definition of sequential and concurrent approaches can be found from (Lu and Kaxiras, 2004). In this paper, a concurrent approach integrating with MBS simulation, explicit FEM analysis, sub-modelling technique as well as crack initiation procedure is developed. A smooth coupling between different scales is organized as below:

1) Complete MBS analysis / Component explicit FEM coupling: To achieve the MBS and explicit FEM hand-shaking, a complete MBS model should be generated firstly. Using the surface crack initiation criteria proposed by (Ekberg et al., 2002), the most critical region over the global track for surface crack to occur will be identified. Following that, a limited length of rail FE model together with a wheel component FE model is produced to simulate the dynamic stress/strain response over the most critical region. The relative contact positions between wheel and rail, wheel running velocities, real-time wheel axle loads obtained from MBS simulation will be transformed into a FE load-vector and applied on the wheel component as dynamic boundary conditions.

2) Component Explicit FEM / Meso – Sub-model coupling: The nodal interface loads (restored in NCFORC result file) obtained from transient wheel-rail explicit FEM analysis will be used as a input for the settlement of coarse full-model boundary conditions. Here, only the rail is considered in the coarse full-model analysis and the nodal interface loads in substitution for the functionality of the wheel are applied on the rail contact patches. After finishing the coarse full-model analysis, refined sub-model as shown in figure 1(c) will be created and its boundary nodes will be stored into a file for displacement interpolation with the full-model result file. The calculated displacement on the cut boundary of the full-model will be used as boundary conditions for sub-modelling analysis. By doing the cut boundary verification and stress-strain post-processing analysis, the coupling between component explicit FEM analysis and sub-modelling simulation will be fulfilled. The validity of the sub-modelling procedure should be further confirmed through comparison with the dynamic simulation results.

3) Meso – Sub-model / Crack initiation analysis coupling: The material planes that are candidate for the maximum damage critical plane is determined by computing the transformation matrices for a given set of angles. The stress tensor and strain tensor at each history point obtained from sub-modelling analysis will be imported to crack initiation procedure. The fatigue parameters defined by critical plane approaches will be computed by rotating the material planes. In the end, the material planes with the maximum fatigue parameters will be viewed as the potential orientation for the crack to initiate.

3 RESULTS AND DISCUSSION

Following the computational multi-scale coupling strategy discussed in section 2, numerical simulations will be implemented at different scales. As a consequence, results and discussions will be presented in this section.

3.1 Complete macro-scale – MBS

In this scale, vehicle bodies, suspensions, subgrade, wheelset represented by springs, dashpots and masses are all assumed to be rigid or elastic bodies. Running through the simulation, it is possible to determine the contact conditions, track load and vehicle stability performance. Typical examples can be found in (Shevtsov, 2008, Wan et al., 2013).

3.1.1 MBS model

A three-dimensional MBS model for a specific Dutch railway curved line is built up in the multi-body simulation software Adams/VI Rail. For the vehicle model, standard Manchester passenger wagon with double wheel-sets in the front and the rear of the car body is utilized, in which the wheel profile is chosen as standard S1002 and the rail profile is UIC54E1. Simulations are implemented with a train speed of 140 km/h over the track, which is considered as a total length of 1000m involving a 400m curved track with the radius of 1000m. The transition region between curves and tangent track is assumed to be 100m.

Regarding the contact mode, General Contact Element (WRGEN) using actual wheel and rail profile to calculate the actual contact kinematics at each simulation step is used in the simulations. WRGEN evaluates the local contact stiffness based on geometry and materials properties.

3.1.2 Dangerous region identification

The fatigue index for surface initiated fatigue is based on the theory of elastic and plastic shakedown in general, and shakedown map theory in particular. The fatigue index is expressed as:

$$FI_{surf} = \mu - \frac{2\pi abk}{3F_z} \quad (1)$$

It is indicated that fatigue may occur if the inequality $FI_{surf} > 0$ is fulfilled. a, b refer to the semi-axes of the Hertzian contact patch and their variations with respect to travelled distance is shown in figure 2 (a-b).

F_z is the normal force magnitude, and k is the yield stress in pure shear. In this study, the traction coefficient μ is defined as,

$$\mu = \frac{F_T}{F_z} = \frac{\sqrt{F_x^2 + F_y^2}}{F_z} \quad (2)$$

Where F_x and F_y are the longitudinal and lateral creep forces, respectively. The variation of traction coefficient with respect to travelled distance is presented in figure 2(c). Following the surface fatigue index presented in formula (1), its variation is displayed in figure 2(d). It can be noticed that the surface fatigue index has already exceeded the critical value of 0, which means there is a great possibility for the surface crack to occur at the curved part ranging from 200m to 650m. Thus, a specific FEM model will be developed in the dangerous region. The simulation results obtained from MBS simulations, such as translation velocities, rotational velocities, vertical wheel loads, will be used as an input for the assignment of FEM model boundaries conditions.

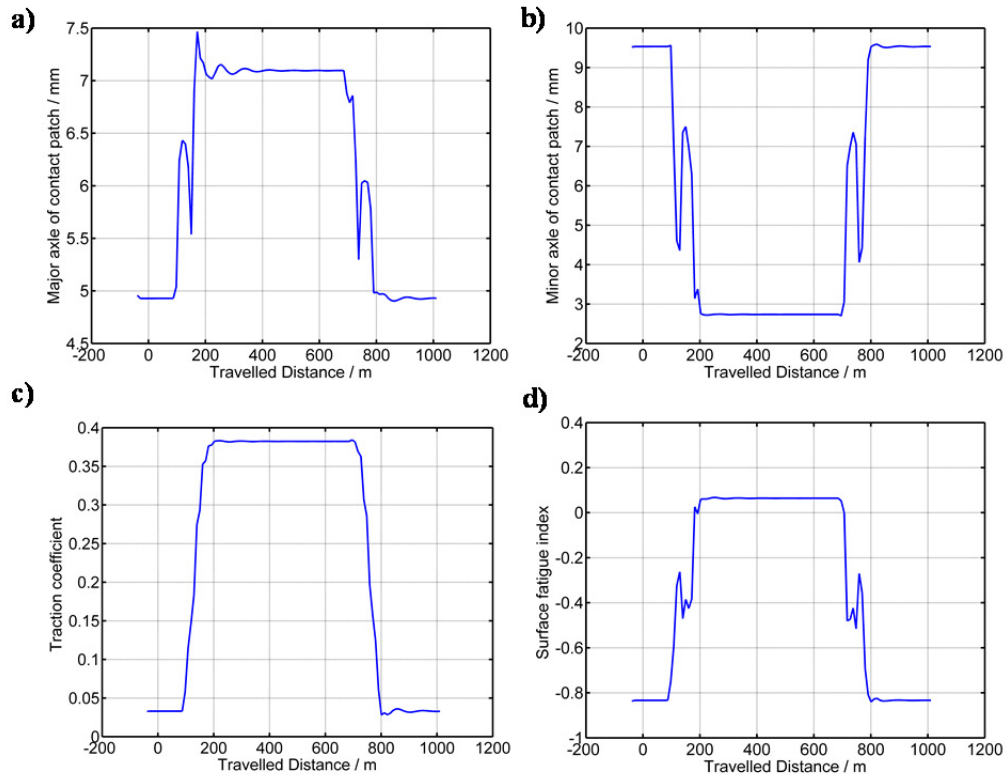


Figure 2. a) Major axle of contact patch; b) minor axle of contact patch; c) traction coefficient; d) surface fatigue index.

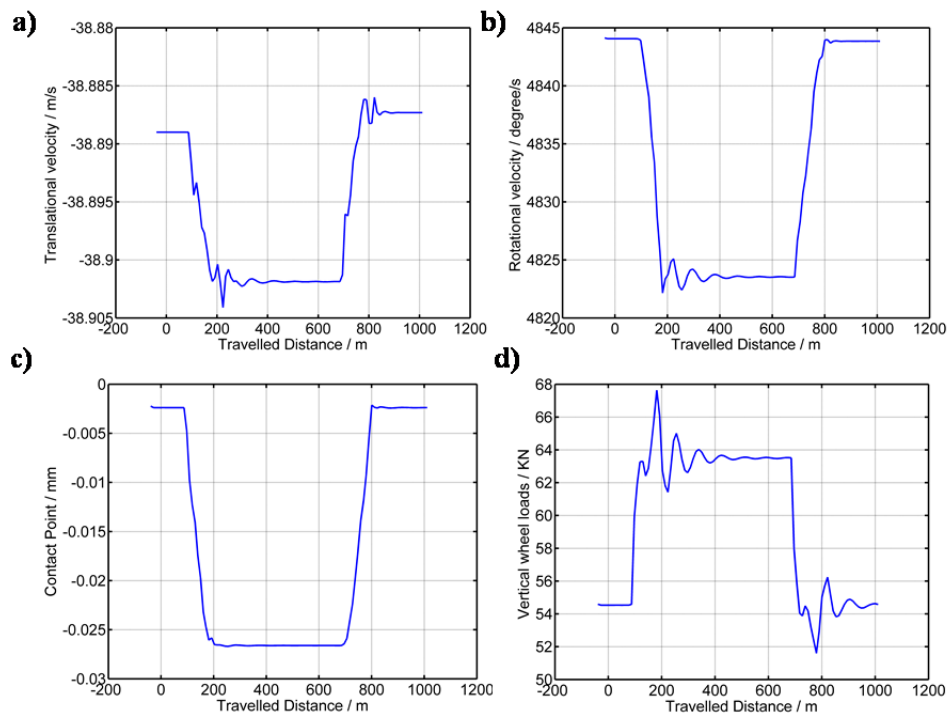


Figure 3. a) Translational velocity; b) Angular velocity; c) Contact point on the rail surface; d) Vertical wheel loads.

3.2 Component macro-scale – explicit FEM

In this scale, the constitutive laws are usually formulated by sophisticated elasto-plastic models so that they can capture the effects on materials properties from lattice defects and microstructural elements. But the boundary conditions settled on the rail and wheel components are postulated to be nominal or equivalent forces and constrains. Representative examples can be seen from (X.Zhao, 2012, Vo et al., 2014, Pletz et al., 2012). FE models and results will be discussed in this section. The details about the numerical procedure can be found in (Ma and Markine, 2015b).

3.2.1 FE model

A three dimensional model, composed of a half wheel and a rail is shown in figure 4. The element size in the solution region is set to be $1.0 \times 1.0 \times 1.0 \text{ mm}$ using the proposed refining method. All together the model consists of 110,000 eight-noded hexahedral solid elements. In the contact region extra care are taken for the elements to be of good quality, while less effort was spent outside the contact region and distorted elements were accepted.

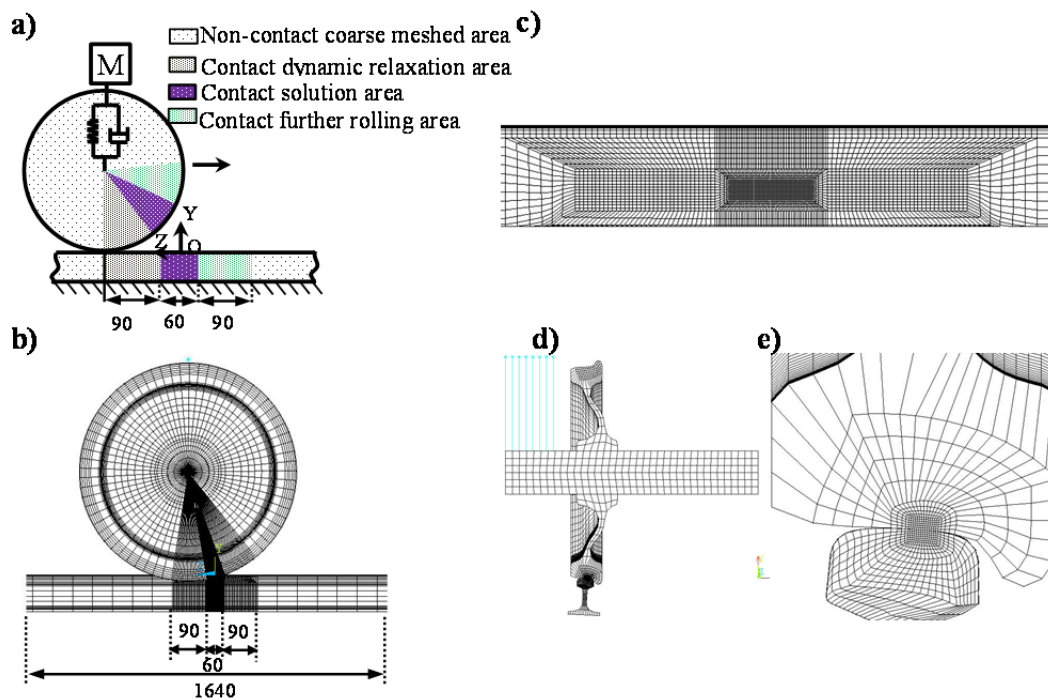


Figure 4. wheel-rail contact dynamic FE model. a) Schematic diagram of FEM; b) FE model – side view; c) Nested mesh at rail refined region; d) FE model – cross sectional; e) Close-up view in the refined contact region.

3.2.2 FEM results

From figure 5, normal contact pressure distribution on the rail surface is observed with a 3D shaded surface plot and 2D contour plot at the origin. In order to demonstrate the surface pressure distribution better, the compressive normal pressure is treated as positive. Due to the non-Hertzian contact conditions, a very high normal contact pressure which amounts to 1010MPa is obtained. The contact patch is not a standard ellipse and asymmetric with respect to its central axis. The length of the contact patch in X and Z direction is 17mm and 14mm respectively. Approximately, the area of the contact patch is 150mm^2 . The reason for the non-elliptical and larger radius contact patch in comparison to literature (X.Zhao, 2012) is attributed to changing radius of curvature of the realistic wheel/rail geometries being in contact as well as the cant angle considered in the model.

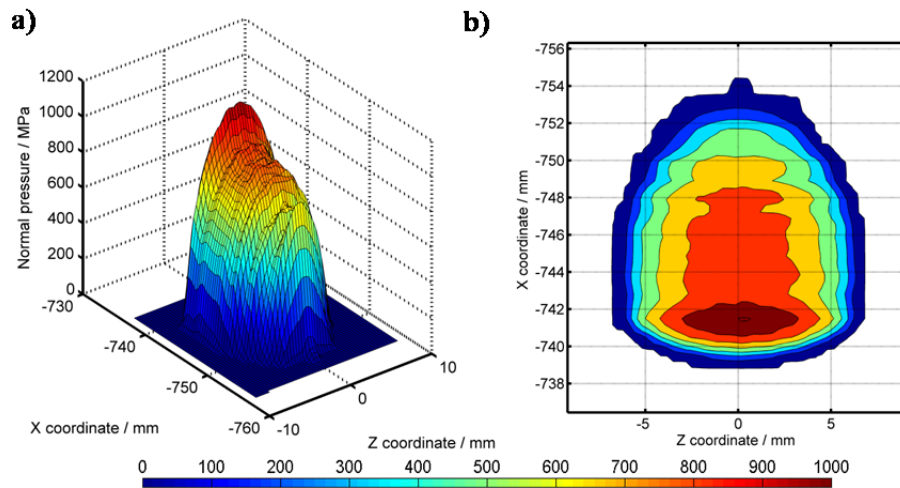


Figure 5. rail surface normal contact pressure distribution at origin $Z = 0$. a) 3D shaded surface plot; b) 2D contour plot.

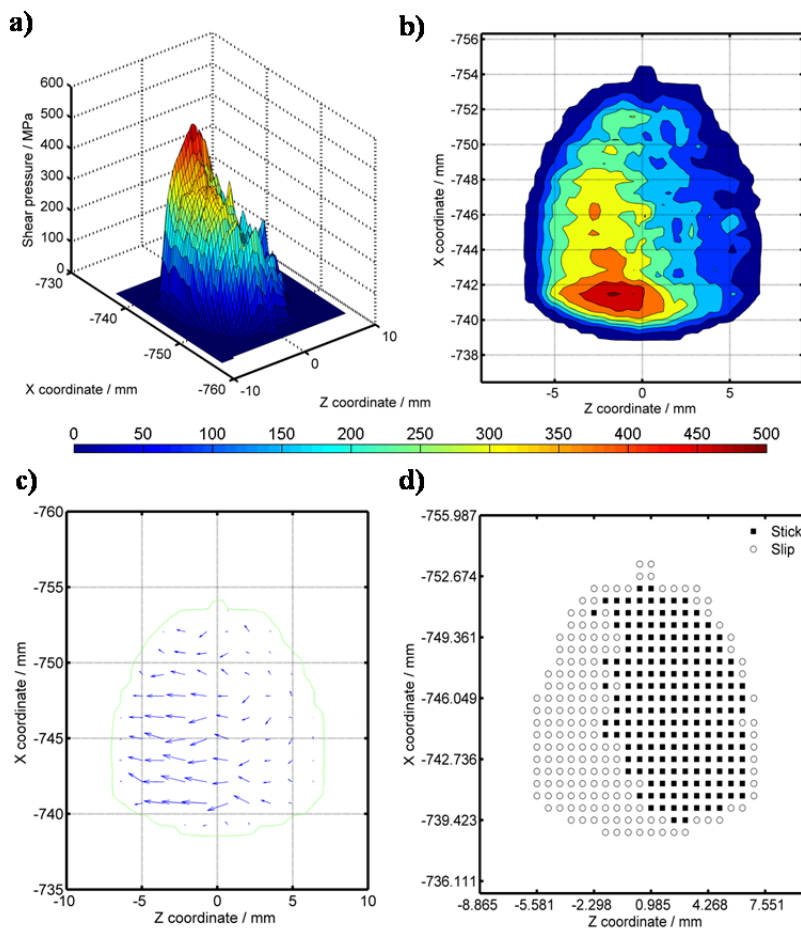


Figure 6. rail surface shear pressure distribution and slip-stick area distribution at origin $Z = 0$ mm. a) 3D shaded surface plot ; b) 2D contour plot; c) Quiver plot; d) Slip-stick area plot.

Accurate estimation of wheel-rail friction levels is of extreme importance in train simulation, since the magnitude of the frictional force on the contact interfaces can determine the crack initiation path and its propagation as well as the development of wear. From figure 5, the distribution of surface shear pressure is observed and it can be seen that

the maximum surface shear pressure amount to as large as 500MPa, which cannot be ignored in comparison to the normal pressure. The surface shear pressure (shown in figure 6(b) contour plot) is mainly distributed at the trailing edge of the contact patch instead of leading edge. The surface shear pressure (shown in figure 6(c) quiver plot) is pointing at the direction of wheel moving, which is logical and consistent with the direction of resultant longitudinal force FZ (shown in figure 5). The criteria for distinguishing the slip and stick area is the same as the one used in (X.Zhao, 2012). As can be seen from figure 6(d), the leading edge of the contact patch is still in stick, whereas the trailing edge is in micro-slip.

In order to check the sub-surface stress response, two cutting surfaces, namely A-A in lateral-vertical plane and B-B in longitudinal-vertical plane, are created. The stresses mapped on the two cutting surfaces are shown in figure (7) (b-c, e-f). For the stress distribution on the A-A cutting surface, the maximum Von Mises stress occurs at the rail top surface and the shear stress exhibits two equal size compressive and tensile components. This phenomenon can be attributed to the contact angle between interfaces, which will lead to a tendency for preventing the wheel sliding away from the rail surface.

While for the stress results on B-B cutting surface, the maximum Von Mises stress moves from sub-surface to the surface caused by the large shear stress at the trailing edge of the contact patch. The tensile and compressive shear stress components are different from the one on A-A cutting surface, which is resulted from the traction moment applied on the wheel axle. The results obtained in this paper is also comparable with reference (Liu et al., 2006).

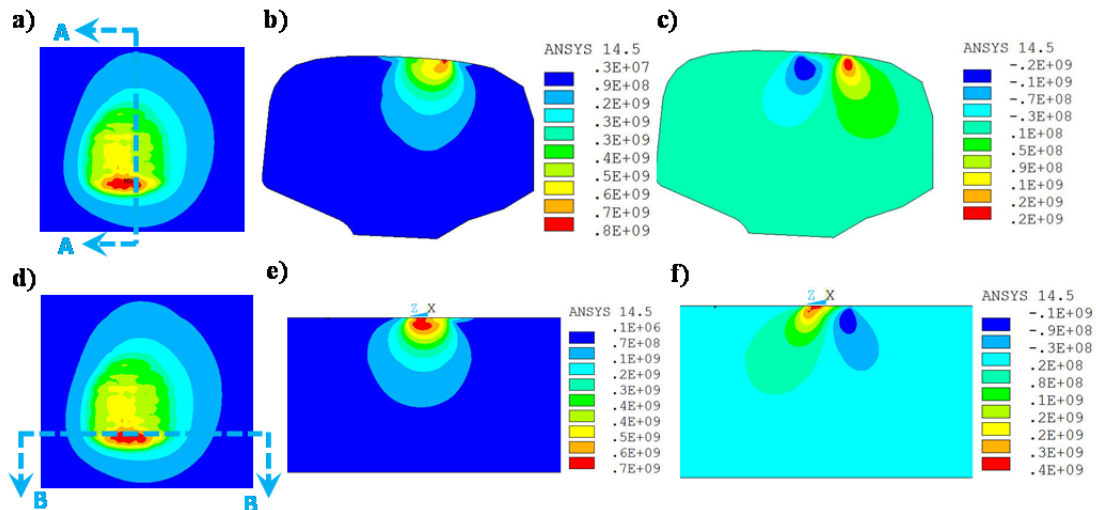


Figure 7. Stress distribution in longitudinal-vertical plane at origin $Z = 0\text{mm}$. a) Cutting surface on X-Y Plane; b) Von-Mises stress on A-A Cutting plane; c) Shear stress on A-A cutting plane; d) Cutting surface on Y-Z Plane; e) Von-Mises stress on B-B Cutting plane; f) Shear stress on B-B cutting plane

3.3 Meso scale – Submodel

Sub-modelling technique known as the cut-boundary displacement method (also known as the specified boundary displacement method) is based on St. Venant's principle, which states: the difference in effects due to two statically equivalent loadings becomes insignificant as the distance from the load application increases. On this scale, sub-modelling approach is often employed to assess the crack initiation on the surfaces of rail and wheel (Liu et al., 2006, Ringsberg et al., 2000, Guagliano and Pau, 2008).

3.3.1 Sub- FE models

While for the full model, it can be observed from figure 8 (a) and (b) that only rail model is considered. The rail dimensions and mesh size remain the same as the one is dynamic

model for applying the nodal interface loads obtained from dynamic simulation results. Regarding sub-model, its dimension is approximately restrained to be block, which is considerably smaller than the dimension of full-model. In order to satisfy the requirement of crack initiation analysis, the mesh size in the sub-model can be refined to 0.2mm, which is five times smaller than the mesh size in full model. Herein, all these three models are discretized by using the nested transition mapped hexahedral refining method, which has already been developed by the presented authors.

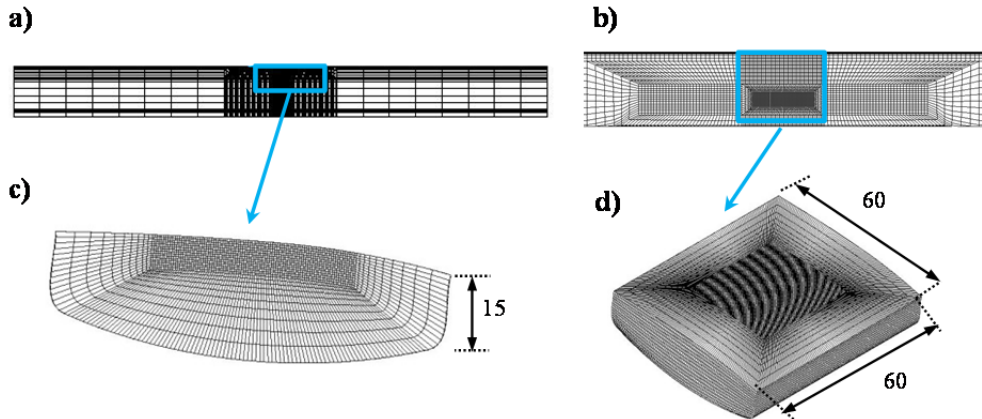


Figure 8. Rail FE model. a) Full-model – side view; b) Full refined region – top view; c) Sub-model – side view; d) Sub-model - isometric view. (Notation: represents the location of sub-model with respect to full model.)

3.3.2 Sub-model results

From figure 9, the comparison of Von Mises stress and shear stress distribution obtained from dynamic model, full-model and sub-model analysis is observed. It can be noticed that the distributions of Von Mises and shear stress from full model and sub-model analysis is almost the same, and only a negligible deviation of the stress amplitude occurs.

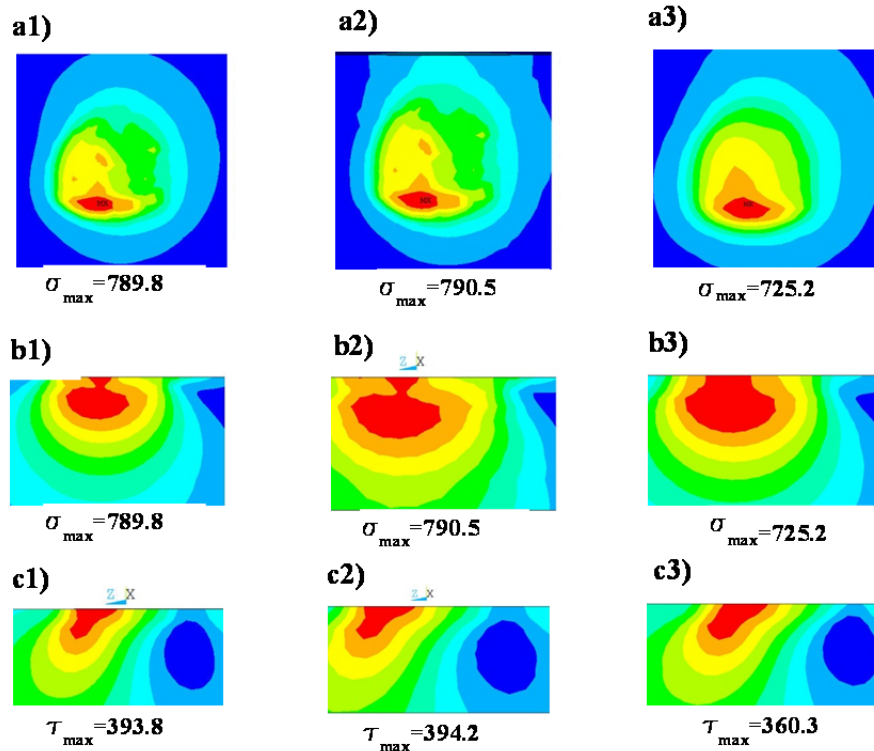


Figure 9. Stress distribution (Unit: MPa) from full-, sub- and dynamic-model. (Notation: “a” represents the Von Mises stress on rail surface from top view; “b” refers to Von Mises stress mapped on the longitudinal-vertical plane; “c” is the shear stress mapped on the longitudinal-vertical plane; “1”, “2” and “3” refer to results from full model, sub model and dynamic model respectively.)

While for the results from dynamic analysis, there is a slight difference on both the stress distribution and its magnitude. The main reason caused the deviation from the dynamic simulation can be attributed to the fact that only the nodal interface applied on the rail full model and no nodal displacement are involved. However, it can be concluded that both the results from the three simulations are comparable, which means the sub-modelling technique is able to be used in wheel-rail contact analysis.

3.4 Crack initiation analysis

It is reported that cracks initiate and grow on certain planes and the normal strains to those planes, assist in the fatigue crack growth process. Base on this phenomenon, different critical plane approaches are proposed to predict the most dangerous plane for the initial crack to grow. In this section, the results for crack initiation analysis will be highlighted and discussed. The details for the crack initiation analysis is available in (Ma and Markine, 2015a).

3.4.1 Critical plane approach

It is postulated that the crack will propagate along the plane of maximum shear strain by Fatemi–Socie (FS model)(Fatemi and Socie, 1988). The fatigue damage parameter is described as formula (3):

$$FP_{\max} = \max_{\Delta} \left[\frac{\Delta\gamma_{\max}}{2} \left(1 + k \frac{\sigma_{n,\max}}{\sigma_y} \right) \right] \quad (3)$$

Where $\Delta\gamma_{\max}$ is the shear strain amplitude on a plane Δ , $\sigma_{n,\max}$ is the maximum normal stress on that plane Δ and k is the material parameter, $k = 1.0$ in this case.

Recently, Jiang & Sehitoglu (JS model) (Jiang and Sehitoglu, 1999) developed an model based on SWT relation. In the model, both the shear stress/strain and normal stress/strain components are used to describe the reason for crack initiation. Its expression is shown as:

$$FP_{\max} = \max_{\Delta} \left(\langle \sigma_{\max} \rangle \frac{\Delta\varepsilon}{2} + J\Delta\gamma\Delta\tau \right) \quad (4)$$

in which $\Delta\tau$ is the shear stress range, $\Delta\gamma$ is the shear strain range. $\langle \rangle$ denotes the MacCauley bracket (i.e. $\langle x \rangle = 0.5(|x| + x)$). J is a load and material-dependent parameter, equal to 0.25 for bainitic alloy or 0.3 manganese steel. Here, to illustrate that is a material constant, we use 0.2 to take the place of J (Ringsberg and Lindbäck, 2003).

3.4.2 Critical plane orientation

Figure 10 shows the contour plot of maximum fatigue parameter under different material plane. Red color means the dangerous material planes for crack initiation, while blue area indicates the safe ones. From red to blue the possibility of crack initiation is gradually decreasing. It can be noticed that the fatigue parameter distribution of FS and JS model is similar but still slight difference exists. That is because that FS model is based on maximum shear strain theory, while JS model is depending on superposition of positive normal strain energy and shear strain energy. Moreover, it can be found from figure 10 (a) that two potential region for crack initiation exists for FS model, when ϕ lies in $[0, 20]$, $[160, 180]$ and θ falls in $[60, 90]$. Regarding JS model, one most dangerous region $\theta \in [0, 20]$, $\phi \in [0, 100]$ occurs. If the contour plots were mapped onto two dimensional rail longitudinal cross section and rail top surface, the potential initial crack orientation can be clearly seen from figure 11. It is indicated that crack will initiate with a deep

angle from the rail surface predicted by FS model. While for JS model, crack may initiate along the path, which will formulate a shallow angle from to with the rail top surface. While for the top view, the two predictions differ from each other even larger.

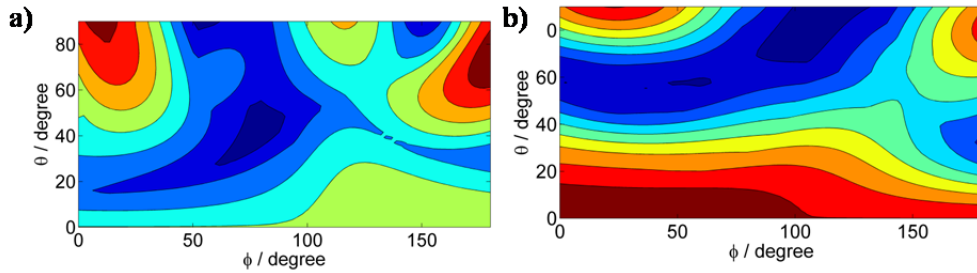


Figure 10. Fatigue parameter variation with plane orientation during one load-cycle. a) FS model; b) JS model. (Color notation: from dark red to dark blue, the possibility of crack initiation is gradually decreasing).

It is not easy to conclude that whether FS model or JS model fits the real W/R contact case, since it is depending more parameters such as material properties, loads etc. Thus, more field tests and experimental research are required to verify the predicting results.

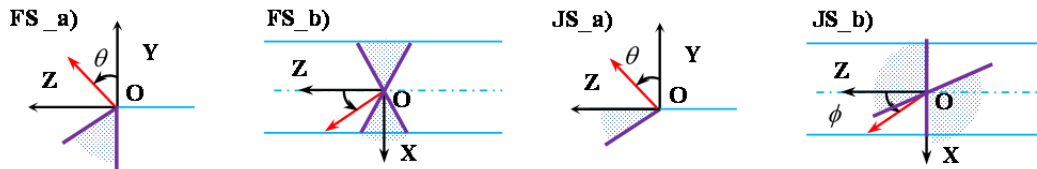


Figure 11. Crack initiation on the rail surface. “a” represents crack orientation on rail longitudinal-vertical cross section; blue line is rail top surface; “b” refers to crack orientation on rail top surface. \dots denotes the potential crack initiation region.

4 CONCLUSION

A computational strategy for rail surface crack initiation analysis is proposed and characterized by a coupling method at different scales. The goal of multi-scale simulation has been achieved with a balance between accuracy, efficiency and realistic description at different length scales. Based on the obtained results, it can be concluded that:

1) In complete macro-scale, an integrated vehicle-track interaction MBS model is developed and utilized to assess the probability of surface crack initiation along a curved track. The relative contact positions, wheel running velocities, real-time wheel axle loads obtained from MBS simulation will be transformed into a FE load-vector and applied on the wheel component as dynamic boundary conditions.

2) In component macro-scale, a dynamic numerical procedure for the wheel and rail rolling contact stress/strain analysis is introduced and characterized by a clear explanation of solving procedure, a novel mesh refinement technique on the wheel/rail contact region. The obtained results, involving stress/strain response and contact pressure distribution as well as contact area, are analyzed and discussed.

3) In mesoscopic scale, a considerable efficiency and accuracy of the simulation results could be obtained with the application of sub-modelling technique. Through the comparison with dynamic- and full- model results, it is confirmed that the sub-modelling procedure is trustworthy and can be used for wheel/rail contact analysis.

4) The crack initiation plane can be varied under different fatigue life models. FS model and JS model are recommended to do the crack initiation analysis on wheel/rail interaction. More field tests and experimental research are required to verify the predicting results.

5 REFERENCE

- BERTOLINO, G., CONSTANTINESCU, A., FERJANI, M. & TREIBER, P. 2007. A multiscale approach of fatigue and shakedown for notched structures. *Theoretical and Applied Fracture Mechanics*, 48, 140-151.
- DESIMONE, H., BERNASCONI, A. & BERETTA, S. 2006. On the application of Dang Van criterion to rolling contact fatigue. *Wear*, 260, 567-572.
- DUBOURG, M. C. & LAMACQ, V. 2002. A predictive rolling contact fatigue crack growth model: Onset of branching, direction, and growth - Role of dry and lubricated conditions on crack patterns. *Journal of Tribology-Transactions of the Asme*, 124, 680-688.
- EKBERG, A., KABO, E. & ANDERSSON, H. 2002. An engineering model for prediction of rolling contact fatigue of railway wheels. *Fatigue & Fracture of Engineering Materials & Structures*, 25, 899-909.
- FATEMI, A. & SOCIE, D. F. 1988. A Critical Plane Approach to Multiaxial Fatigue Damage Including out-of-Phase Loading. *Fatigue & Fracture of Engineering Materials & Structures*, 11, 149-165.
- FRANKLIN, F. J., GAHLOT, A., FLETCHER, D. I., GARNHAM, J. E. & DAVIS, C. 2011. Three-dimensional modelling of rail steel microstructure and crack growth. *Wear*, 271, 357-363.
- GUAGLIANO, M. & PAU, M. 2008. An experimental–numerical approach for the analysis of internally cracked railway wheels. *Wear*, 265, 1387-1395.
- JIANG, Y. & SEHITOGLU, H. 1999. A model for rolling contact failure. *Wear*, 224, 38-49.
- LI, X., YANG, J. Z. & WEINAN, E. 2010. A multiscale coupling method for the modeling of dynamics of solids with application to brittle cracks. *Journal of Computational Physics*, 229, 3970-3987.
- LIU, Y., STRATMAN, B. & MAHADEVAN, S. 2006. Fatigue crack initiation life prediction of railroad wheels. *International Journal of Fatigue*, 28, 747-756.
- LU, G. & KAXIRAS, E. 2004. An overview of multiscale simulations of materials. *arXiv preprint cond-mat/0401073*.
- MA, Y. & MARKINE, V. L. 2015a. Numerical Analysis for Fatigue Life Prediction on Railroad RCF Crack Initiation. *10th International Conference on Contact Mechanics*. Colorado.
- MA, Y. & MARKINE, V. L. 2015b. A Numerical Procedure for Analysis of W/R Contact Using Explicit Finite Element Methods. *10th International Conference on Contact Mechanics*. Colorado.
- PLETZ, M., DAVES, W. & OSSBERGER, H. 2012. A wheel set/crossing model regarding impact, sliding and deformation—Explicit finite element approach. *Wear*, 294-295, 446-456.
- RINGSBERG, J. W. & LINDBÄCK, T. 2003. Rolling contact fatigue analysis of rails including numerical simulations of the rail manufacturing process and repeated wheel-rail contact loads. *International Journal of Fatigue*, 25, 547-558.
- RINGSBERG, J. W., LOO-MORREY, M., JOSEFSON, B. L., KAPOOR, A. & BEYNON, J. H. 2000. Prediction of fatigue crack initiation for rolling contact fatigue. *International Journal of Fatigue*, 22, 205-215.
- SHEVTSOV, I. Y. 2008. *Wheel/rail interface optimisation*. PhD, Delft university of technology.
- SRAML, M., FLA KER, J. & POTR, I. 2003. Numerical procedure for predicting the rolling contact fatigue crack initiation. *International Journal of Fatigue*, 25, 585-595.
- STEENBERGEN, M. & DOLLEVOET, R. 2013. On the mechanism of squat formation on train rails – Part I: Origination. *International Journal of Fatigue*, 47, 361-372.
- VO, K. D., TIEU, A. K., ZHU, H. T. & KOSASIH, P. B. 2014. A 3D dynamic model to investigate wheel–rail contact under high and low adhesion. *International Journal of Mechanical Sciences*, 85, 63-75.
- WAN, C., MARKINE, V., SHEVTSOV, I. & DOLLEVOET, R. 2013. Improvement of train-track interaction in turnouts by optimising the shape of crossing nose.
- X.ZHAO. 2012. *Dynamic Wheel/Rail Rolling Contact at Singular Defects with Application to Squats*. PhD, Delft university of technology.
- YANG, D., ZHANG, H., ZHANG, S. & LU, M. 2014. A multiscale strategy for thermo-elastic plastic stress analysis of heterogeneous multiphase materials. *Acta Mechanica*, 1-21.